AIP | Applied Physics Letters

Asymmetric wicking and reduced evaporation time of droplets penetrating a thin double-layered porous material

Amir D. Gat, Aria Vahdani, Homayun Navaz, Albert Nowakowski, and Morteza Gharib

Citation: Appl. Phys. Lett. **103**, 134104 (2013); doi: 10.1063/1.4823534
View online: http://dx.doi.org/10.1063/1.4823534
View Table of Contents: http://apl.aip.org/resource/1/APPLAB/v103/i13
Published by the AIP Publishing LLC.

Asymmetric wicking and reduced evaporation time of droplets penetrating a thin double-layered porous material

Amir D. Gat,[1,a)] Aria Vahdani,[2] Homayun Navaz,[3] Albert Nowakowski,[3] and Morteza Gharib[2]
[1]*Faculty of Mechanical Engineering, Technion-Israel Institute of Technology, Haifa 32000, Israel*
[2]*Graduate Aerospace Laboratories, California Institute of Technology, Pasadena, California 91125, USA*
[3]*Faculty of Mechanical Engineering, Kettering University, Flint, Michigan 48504, USA*

(Received 24 July 2013; accepted 12 September 2013; published online 26 September 2013)

We study numerically and experimentally the penetration and evaporation dynamics of droplets wicking into a thin double-layered porous material with order-of-magnitude difference in the physical properties between the layers. We show that such double-layered porous materials can be used to create highly asymmetrical wicking properties, preventing liquid droplets wicking from one surface to the other, while allowing wicking in the reverse direction. In addition, these double-layered porous materials are shown to reduce the evaporation time of droplets penetrating into the porous material, compared with a single-layered porous material of equal thickness and physical properties similar to either of the layers. © *2013 AIP Publishing LLC*.
[http://dx.doi.org/10.1063/1.4823534]

The penetration and evaporation dynamics of droplets wicking into porous materials is relevant to various applications such as spreading of contamination, spreading of stains or sweat in fabrics, coating processes, and ink-jet printing. Current methods to create breathable fabrics include hydrophobic materials and prevent both liquid penetration and exit from the fabric (e.g., Gor-Tex hydrophobic durable water repellent (DWR) coating) while only allowing for vapor transfer. We suggested utilizing double-layered porous material to create asymmetric wicking properties allowing for fabrication of hydrophilic fabrics which prevent liquid (such as hazardous chemicals) to come in contact with the skin while allowing for exit of droplets (such as sweat droplets) from the skin and accelerate liquid evaporation.

Following deposition onto a porous surface, the droplet spread is driven by the capillary pressures, and (for volatile liquids) evaporation occurs both from the surface of the droplet outside the porous medium and from inside the pores where the liquid phase resides.[1–3] Extensive studies focused on the spreading dynamics of droplets wicking into porous surfaces.[2,4–9] Clarke *et al.*[10] developed a theoretical model for the spreading and imbibition of droplets into porous surfaces. D'Onofrio *et al.*[11] and Markicevic *et al.*[12] studied the spreading of a sessile droplet into sand, utilizing both numerical and experimental methods. Alleborn and Raszillier[13] studied numerically the spreading and sorption of a droplet into single and double-layered porous surfaces and suggested a model for wicking into thin porous surfaces. Gerlach *et al.*[14,15] studied numerically the spreading dynamics of droplets into unsaturated layered porous surfaces with identical capillary pressure drop. Similarly, Varlamov *et al.*[16] studied a two-dimensional absorption of a micro-droplet into a two-layered substrate by experimental and numerical methods. The results in Ref. 16 presented a relation between the ratio of the pore size of the layers and the wicking time and liquid distribution within the porous material.

We study the wicking and evaporation dynamics of a droplet penetrating into a thin double-layered porous material with order-of-magnitude difference in physical properties between the layers. Our work focuses on asymmetry in wicking and evaporation dynamics by comparing the liquid distribution between the layers and rate of evaporation for a droplet wicking from one side of the double-layered material versus a droplet entering from the opposite direction. We show experimentally and numerically that such double-layered materials can be used to achieve asymmetric penetration dynamics and to reduce the droplet evaporation time (compared to single layered porous materials), which may be of interest to applications such as breathable fabrics and medical bandages.

We denote the layer close to the skin as the inner-layer and the layer far from the skin as the outer-layer (see Figure 1). Hereafter, the subscript n marks the inner-layer ($n=i$) or outer-layer ($n=o$) property. The relevant parameters are the layer width h_n, permeability k_n, capillary pressure drop p_n, porosity ϕ_n, droplet volume V, viscosity μ, and time t.[7,16,17] The flow within the porous material is governed by the phenomenological Darcy's law[18]

$$\mathbf{u} = -\frac{k_n}{\mu\phi_n}\nabla p, \tag{1}$$

where $\mathbf{u}$ is the velocity.

We require that a droplet of volume V positioned on the outer-layer (see Figure 1) would not penetrate through the width of the inner-layer, while allowing for droplets positioned on the inner-layer to wick into the outer-layer. In order to achieve this we require that the characteristic time for full penetration of the droplet into the outer-layer is order-of-magnitude smaller than the characteristic time required for penetration through the width of the inner-layer. We denote the

[a)]amirgat@tx.technion.ac.il

characteristic time for full wicking of the droplet into the outer-layer as t_o and the time required to penetrate h_i as t_i. The characteristic length scale of the imprint of the liquid in the outer-layer, denoted as l_o, can be estimated from conservation of mass as $l_o \sim O(\sqrt{V}/\sqrt{h_o}\phi_o\pi)$. We can estimate the pressure gradient in the radial direction as $\partial p/\partial r \sim O(p_o/l_o)$, and thus from Eq. (1) the time scale t_o for full penetration of the droplet into the outer-layer is estimated as $t_o \sim O(V\mu/\phi_o h_o \pi^2 2k_o p_o)$. Similarly, the time scale for penetration of liquid through the inner-layer width is estimated as $t_i \sim O(h_i^2 \mu\phi_i/2k_i p_i)$, where the characteristic length is h_i and pressure gradient is $\partial p/\partial z \sim O(p_i/h_i)$. We require $t_o \ll t_i$, yielding the condition

$$\frac{t_o}{t_i} = \frac{V}{\phi_o h_o \pi^2 h_i^2 \phi_i}\frac{k_i p_i}{k_o p_o} \ll 1. \quad (2)$$

Provided Eq. (2) is satisfied, the droplet would fully penetrate into the outer-layer order-of-magnitude faster than the time required to penetrate the width of the inner-layer, and thus the inner surface would remain dry throughout the primary wicking phase. Additional requirement is that the capillary pressure drop at the outer-layer is order-of-magnitude greater than the capillary pressure drop at the inner-layer, $p_i \ll p_o$, and thus the full penetration of the droplet into the porous material would be limited to the outer-layer as $t \to \infty$. For a droplet positioned on the inner-layer the initial wicking will be within the inner-layer. However, after initial spreading in the inner-layer and contact of the liquid with the interface between the layers, and since the time scale for wicking into the outer-layer is order-of-magnitude smaller than the inner-layer, the liquid will wick primarily into the outer-layer, and its imprint on the inner-layer is thus determined by the imprint at the time of contact of the liquid with the outer-layer.

We performed experiments with two types of hydrophilic nylon membranes (Scientific Tisch, TM) with order-of-magnitude difference in, r_n, the average pore radius ($r_n = 5\,\mu$m and $0.1\,\mu$m) and identical porosity ($\phi_i \approx \phi_o \approx 0.2$) and thickness ($h_i = h_o = 100\,\mu$m). The permeability of the layers is proportional to $k_n \propto r_n^2$ (Ref. 19), and the pressure drop due to capillary forces is proportional to $\propto \delta/r_n$, where δ is the surface tension of the liquid, and thus the membranes can be used to create a double-layered porous material with an order-of-magnitude difference in the capillary pressure drop between the layers. For each combination of layers 10 identical experiments were conducted.

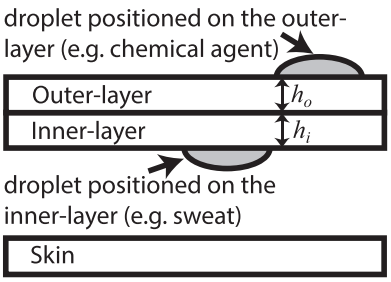

FIG. 1. Illustration of double-layered fabric with liquid droplets on the inner- and outer-layers.

We examined the mass distribution between the layers of a 40 μl de-ionized water droplet positioned on the inner-layer ($r_i = 5\,\mu$m) or outer-layer ($r_o = 0.1\,\mu$m), see Figure 1. The de-ionized water is characterized by density $\rho = 10^3 \text{kg/m}^3$, viscosity $\mu = 10^{-3}\text{Pa} \times \text{s}$, surface tension $\delta = 0.072\text{N/m}$, and negligible contact angle with the porous surface $\alpha \approx 0$. When a droplet was positioned on the outer-layer, 99% of the liquid mass remained in the outer-layer, with standard deviation of 5%, and thus the liquid did not penetrate into the inner-layer (as illustrated in Figure 2(a)). For the opposite case, where a liquid droplet is positioned on the inner-layer (e.g., sweat droplet), 57% of the liquid was transferred to the outer-layer (as illustrated in Figure 2(b)), with standard deviation of 7%. Two control experiments were conducted in order to support our claim that the difference is caused by the different values of the capillary pressure drop. In the first experiment, both layers had an identical pore size of 5 μm. A droplet was positioned on the outer-layer, and 54% of the liquid remained on the outer-layer while the rest traveled through to the inner-layer with a standard deviation of 22%. In the second experiment, both layers had an identical pore size of 0.1 μm. For this case 55% of the liquid remain on the outer-layer with a standard deviation of 20%.

In addition, we examined the effect such double-layered porous materials on the rate of evaporation. The layering of the porous material creates a preference for one layer over the other, and thus the liquid is expected to have a larger contact area with the surrounding air. This increase in surface area reduces the time required for evaporation. The evaporation time of a 200 μl ethanol droplet positioned on a double-layered porous material is presented in Figure 4, where four combinations of inner- and outer-layer pore sizes are examined and compared with numerical computations. The ethanol droplet is characterized by density $\rho = 789\,\text{kg/m}^3$, viscosity $\mu = 1.07 \times 10^{-3}\text{Pa} \times \text{s}$, surface tension $\delta = 0.022\text{N/m}$, and negligible contact angle with the porous surface $\alpha \approx 0$. In all cases the droplet is positioned on the inner-layer, and the inner-layer is positioned over a glass surface while the outer-layer is exposed. The double-layered material was positioned on a scale, and the reduction of the mass of the liquid over time was measured. While evaporation occurs from both the surface of the droplet and from the liquid within the porous material, the characteristic time for droplet penetration is 1 s, which is negligible compared with the 100 s characteristic time for evaporation of the ethanol droplet. Thus, the measurements represent the evaporation of liquid from within the

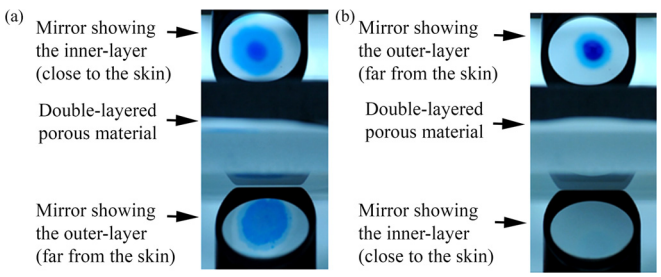

FIG. 2. Experimental illustration of asymmetric wicking in thin double-layered porous materials. The inner-layer average pore size is 5 μm, and the outer-layer average pore size is 0.1 μm. In case (a) a droplet is positioned on the inner-layer while in case (b) a droplet is positioned on the outer-layer.

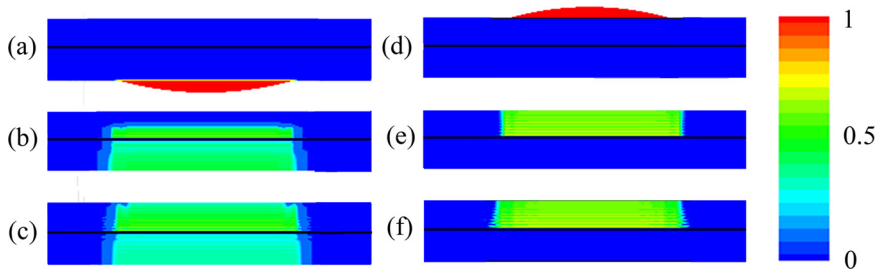

FIG. 3. Numerical computations based image of liquid transport and spread through a double-layer porous material at various times. In all cases the upper layer is the outer-layer, and the lower layer is the inner-layer. The droplet is positioned on the inner-layer in (a)–(c) and on the outer-layer in (d)-(f). The image is stretched ×8 in the vertical direction in order to increase the clarity of the images.

porous material. The case in which the outer-layer pore size is order-of-magnitude smaller than the inner-layer pore size reduced the evaporation time at ≈50% compared to all other cases (see Figure 4), thus suggesting that such a combination can be used to increase the evaporation rate for droplets positioned on the inner-layer (e.g., sweat droplets).

We conducted numerical computations in order to simulate a double-layered material with order-of-magnitude difference in pore size between the layers, similarly to the experiments, and study the behavior of a droplet penetrating and spreading inside the material. Hereafter, the subscripts l and g refer to liquid and gas phases, respectively. The subscript j refers to jth gaseous constituent (air and liquid vapor phase in this case), and variables without reference to each constituent are properties of the mixture. The mass and momentum conservation equations for a wetting and non-wetting multi-fluids (liquid and gas) are[20]

$$\frac{\partial(\phi\rho_l s_l)}{\partial t} + \nabla\cdot(\phi\rho_l s_l \mathbf{u}_l) = -\dot{\rho}_l^{se} - \dot{\rho}_l^{su}, \tag{3}$$

where $\mathbf{u}_l$ is the liquid velocity, defined by Eq. (1) as $\mathbf{u}_l = -Kk_l/\mu_l(\nabla p_l - \rho_l g s_l)$ and

$$\frac{\partial(\phi\rho_g s_g)}{\partial t} + \nabla\cdot(\phi\rho_{gj} s_g \mathbf{u}_{gj}) = \dot{\rho}_l^{se}, \tag{4}$$

where $\mathbf{u}_{gj}$ is the velocity of the jth gas constituent, defined by Eq. (1) as $\mathbf{u}_{gj} = -Kk_{gj}/\mu_g(\nabla p_{gj} - \rho_{gj} g s_g) - D_{j\to mix}\nabla C_{gj}$, K is saturation permeability, μ_l is liquid viscosity, k_l is relative permeability of the liquid phase, ρ_l is density of the liquid, ϕ_n is porosity, $\dot{\rho}_l^{su}$ is evaporation rate at the liquid surface, $\dot{\rho}_l^{se}$ is secondary evaporation, g is gravity, s is saturation ($s_g = 1 - s_l$), $\rho_g = \sum \rho_{gj} C_{gj}$ is the gas density, $C_{gj} = \rho_{gj}\rho_g$ is the mass fraction of the jth gas constituent, k_{gj} is the relative permeability of the jth gas constituent, $\mu_g = \sum \mu_{gj} C_{gj}$ is the gas mixture viscosity, and ρ_{gj} is the density of the jth gas constituent. Equations (3) and (4) were transformed into the computational domain $[\xi = \xi(x,y,z),\ \eta = \eta(x,y,z),\ \zeta = \zeta(x,y,z)]$ and marched in time to obtain the saturation function via the explicit fourth-order Runge-Kutta.[21] At the boundary between the droplet and the porous substrate, the liquid saturation is unity ($s_l = 1$), and the capillary pressure is enhanced by the local hydrostatic pressure (based on local height, h^* of the sessile droplet). Mass is being transported into the porous medium according to $(\rho_l v\phi)/J$, where J is the Jacobian for the transformation and v is the contra-variant vertical velocity given by $\mathbf{u} = \eta_x u + \eta_y v + \eta_z w$ with u, v, w being the three components of the velocity and η_x, η_y, η_z being the metrics for the transformation. The mass transfer is calculated in each time step, and the instantaneous remaining mass yields the liquid bridge volume. This model has been extensively validated by previous studies.[20–22]

We simulated a 40 μl de-ionized water droplet positioned on the outer-layer and on the inner-layer. The evaporation module was activated to monitor the vapor concentration as well as liquid saturation. The difference in pore size yields difference in the capillary pressures between the outer-layer and the inner-layer ($p_o \gg p_i$) and creates asymmetry in wicking properties for a droplet positioned on the inner- and outer-layers. Figure 3 shows the saturation distribution of a water droplet positioned on the inner-layer (a) and the outer-layer (b). In accordance with the experimental data, the droplet positioned on outer-layer did not wick into the inner-layer, while the droplet positioned on the inner-layer significantly wicked into the outer-layer. The vapor phase also followed a similar pattern (see Figure 4), and for the case in which the droplet was positioned on the outer-layer, the amount of vapor in the inner-layer is shown to be order of magnitude

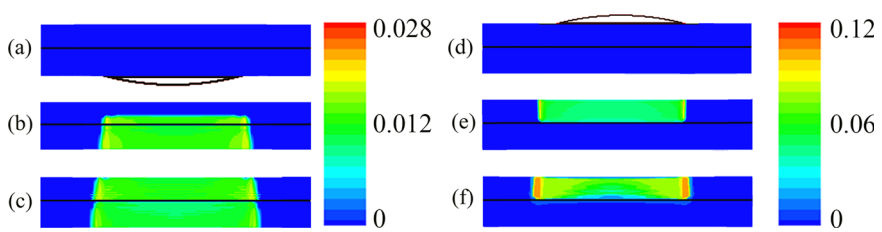

FIG. 4. Numerical computations based image of the vapor transport and spread in the outer- and inner-layers. In all cases the upper layer is the outer-layer, and the lower layer is the inner-layer. The droplet is positioned on the inner-layer in (a)–(c) and on the outer-layer in (d)–(f). The image is stretched ×8 in the vertical direction in order to increase the clarity of the images.

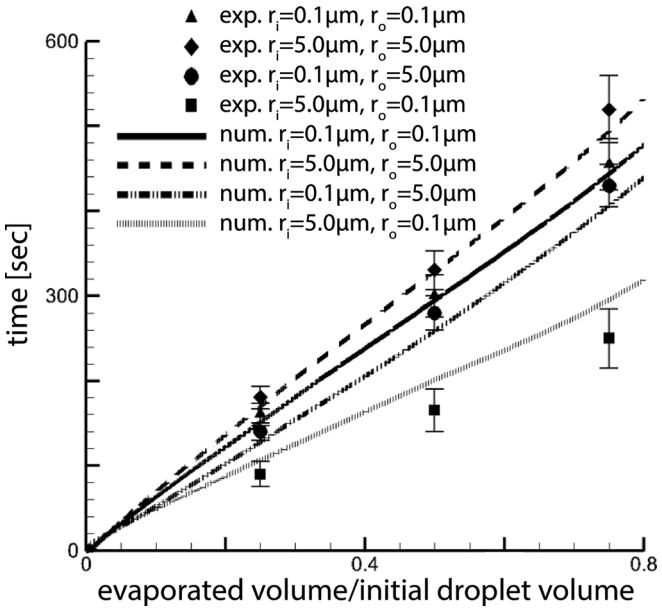

FIG. 5. Numerical and experimental evaporation vs. time for 200 μl ethanol droplet, positioned on the inner-layer of various combinations of nylon membranes (Scientific Tisch, TM) with 5 μm and 0.1 μm average pore size.

smaller than the vapor in the outer-layer, implying that the capillary pressure difference between the two layers can be also utilized as a tool to prevent volatile chemicals to reach to skin.

In addition, we simulated the evaporation of a 200 μl ethanol droplet initially positioned on the inner-layer. Figure 5 presents the experimental and numerical predictions for all examined combinations of the inner-layer and outer-layer pore sizes. Similarly to the experimental data, the evaporation time for the case in which $p_o \gg p_i$ is shown to be reduced by $\approx$40% (see Figure 5), compared to the case $p_i \gg p_o$ and compared to a control single-layer material with the properties of either of the layers.

In conclusion, by utilizing an order-of-magnitude difference in the capillary pressure drop between two thin porous layers (achieved by selecting layers with different chemical properties or different pore sizes) a diodic effect is shown to be obtained where the wicking geometry in one direction is significantly different from the wicking in the opposite direction. While the experimental and numerical results of the current study are limited to asymmetry created by order-of-magnitude difference in pore size, order-of-magnitude analysis (see Figure 2) suggests that other parameters, such as contact angle, permeability, and porosity, can be used to create asymmetric double-layered materials. In addition, the concept presented in this work can be generalized to porous materials with complex spatially varying pore sizes which will enable more complex control over wicking and evaporation processes of droplets.

Double-layered porous materials can be utilized to fabric and bandage applications by preventing penetration of external droplets (e.g., hazardous liquid) and their contact with the skin while allowing droplets to be transferred from the skin (e.g., sweat) to the outer-layer. Furthermore, it was experimentally and numerically demonstrated that double-layered materials can increase the rate of evaporation of droplets positioned on the inner-layer which may be of interest to fabric design. While current methods to create breathable fabrics include hydrophobic materials and prevent both liquid penetration and exit from the fabric (e.g., Gor-Tex hydrophobic DWR coating), double-layered fabrics can be based on hydrophilic porous materials and allow exit of both vapor and liquid while preventing penetration of droplets from the outer-layer.

This work was supported by the Defense Threat Reduction Agency (DTRA) and Cheryk Laboratory for Bio-inspired Engineering at Caltech.

[1]N. C. Reis, Jr., R. F. Griffiths, M. D. Mantle, and L. F. Gladden, Int. J. Heat Mass Transfer **46**, 1279 (2003).
[2]A. Zadrazil, F. Stepanek, and O. Matar, J. Fluid Mech. **562**, 1 (2006).
[3]N. Nikolopoulos, A. Theodorakakos, and G. Bergeles, Int. J. Heat Mass Transfer **50**, 303 (2007).
[4]S. Davis and L. Hocking, Phys. Fluids **12**, 1646 (2000).
[5]R. Holman, M. Cima, S. Uhland, and E. Sachs, J. Colloid Interface Sci. **249**, 432 (2002).
[6]V. Starov, S. Kostvintsev, V. Sobolev, M. Velarde, and S. Zhdanov, J. Colloid Interface Sci. **252**, 397 (2002).
[7]R. Daniel and J. Berg, Adv. Colloid Interface Sci. **123**, 439–469 (2006).
[8]P. Alam, M. Toivakkaa, K. Backfolkb, and P. Sirviob, Chem. Eng. Sci. **62**, 3142 (2007).
[9]A. Gat, H. Navaz, and M. Gharib, J. Fluid Mech. **703**, 315 (2012).
[10]A. Clarke, T. Blake, K. Carruthers, and A. Woodward, Langmuir **18**, 2980 (2002).
[11]T. G. D'Onofrio, H. K. Navaz, B. Markicevic, B. A. Mantooth, and K. B. Sumpter, Langmuir **26**, 3317 (2009).
[12]B. Markicevic, T. G. D'Onofrio, and H. K. Navaz, Phys. Fluids **22**, 012103 (2010).
[13]N. Alleborn and H. Raszillier, J. Colloid Interface Sci. **280**, 449 (2004).
[14]D. Gerlach and N. Alleborn, *13th International Coating Science and Technology Symposium* (Denver, Colorado, 2006).
[15]D. Gerlach, N. Alleborn, H. Raszillier, and A. Delgado, Proc. Appl. Math. Mech. **7**, 4100015 (2007).
[16]Y. Varlamov, Y. Meshcheryakov, M. Predtechensky, and S. Ulyankin, J. Appl. Mech. Tech. Phys. **48**, 101 (2007).
[17]P. G. De Gennes, *F. Brochard-Wyart, and Quéré, Capillarity and Wetting Phenomena: Drops, Bubbles, Pearls, Waves* (Springer-Verlag, New York, 2004).
[18]H. P. G. Darcy, *Les fontaines publiques de la ville de Dijon* (Dalmont, Paris, 1856).
[19]G. S. Beavers and D. D. Joseph, J. Fluid Mech. **30**, 197 (1967).
[20]H. K. Navaz, A. Zand, T. Atkinson, A. Nowakowski, J. Kiple, K. Kamensky, and Z. Jovic, "Agent fate modeling, theory and analysis Volume I," Technical Report, Edgewood Chemical and Biological Center (ECBC), 2013.
[21]H. K. Navaz, B. Markicevic, A. R. Zand, Y. Sikorski, E. Chan, M. Sanders, and T. G. D'Onofrio, J. Colloid Interface Sci. **325**, 440 (2008).
[22]J. L. Regens, J. T. Gunter, M. Amin, A. Nowakowski, and H. Navaz, Hum. Ecol. Risk Asses. **17**, 1229 (2011).